

## Macroscopic complexity from an autonomous network of networks of theta neurons

Tanushree B. Luke, Ernest Barreto and Paul So

Journal Name: Frontiers in Computational Neuroscience  
ISSN: 1662-5188  
Article type: Original Research Article  
Received on: 31 Aug 2014  
Accepted on: 27 Oct 2014  
Provisional PDF published on: 27 Oct 2014  
www.frontiersin.org: [www.frontiersin.org](http://www.frontiersin.org)  
Citation: Luke TB, Barreto E and So P(2014) Macroscopic complexity from an autonomous network of networks of theta neurons. *Front. Comput. Neurosci.* 8:145. doi:10.3389/fncom.2014.00145  
Copyright statement: © 2014 Luke, Barreto and So. This is an open-access article distributed under the terms of the [Creative Commons Attribution License \(CC BY\)](http://creativecommons.org/licenses/by/2.0/). The use, distribution and reproduction in other forums is permitted, provided the original author(s) or licensor are credited and that the original publication in this journal is cited, in accordance with accepted academic practice. No use, distribution or reproduction is permitted which does not comply with these terms.

This Provisional PDF corresponds to the article as it appeared upon acceptance, after rigorous peer-review. Fully formatted PDF and full text (HTML) versions will be made available soon.



1

# Macroscopic complexity from an autonomous network of networks of theta neurons

Tanushree B Luke Ernest Barreto and Paul So \*

*School of Physics, Astronomy, and Computational Sciences and The Krasnow Institute for Advanced Study, George Mason University, Fairfax Virginia 22030, USA*

Correspondence\*:

Paul So

Mail Stop 2A1, George Mason University, Fairfax Virginia 22030, USA,  
paso@gmu.edu

## 2 ABSTRACT

3 We examine the emergence of collective dynamical structures and complexity in a network  
4 of interacting populations of neuronal oscillators. Each population consists of a heterogeneous  
5 collection of globally-coupled theta neurons, which are a canonical representation of Type-1  
6 neurons. For simplicity, the populations are arranged in a fully autonomous driver-response  
7 configuration, and we obtain a full description of the asymptotic macroscopic dynamics of this  
8 network. We find that the collective macroscopic behavior of the response population can exhibit  
9 equilibrium and limit cycle states, multistability, quasiperiodicity, and chaos, and we obtain detailed  
10 bifurcation diagrams that clarify the transitions between these macrostates. Furthermore,  
11 we show that despite the complexity that emerges, it is possible to understand the complicated  
12 dynamical structure of this system by building on the understanding of the collective behav-  
13 ior of a single population of theta neurons. This work is a first step in the construction of a  
14 mathematically-tractable network-of-networks representation of neuronal network dynamics.

15 **Keywords:** theta neuron, type-I neuron, hierarchical network, neural field, macroscopic behavior, coherence, synchrony, chaos

## 1 INTRODUCTION

16 The brain is a complex hierarchical network of networks (**Bullmore and Sporns (2009); Meunier et al.**  
17 **(2010); Zhou et al. (2006)**). Neurons are organized into different neuronal assemblies, and these neuronal  
18 assemblies interact with each other, forming larger assemblies (**Sherrington (1906); Hebb (1949); Har-**  
19 **ris (2005)**). But while there is a wealth of knowledge on the microscopic scale regarding the dynamics  
20 of individual neurons, the macroscopic behavior of such interacting populations of neurons is not well  
21 understood. Indeed, the functional and information-processing activity of the brain, from perception to  
22 consciousness, is thought to result from the emergent collective behavior of these assemblies.

23 In recent years, the mathematical study of networks of this kind, based on globally-coupled popula-  
24 tions of simple phase oscillators, has advanced significantly. This is in large part due to new analytical  
25 techniques (**Ott and Antonsen (2008, 2009); Marvel et al. (2009); Pikovsky and Rosenblum (2011);**  
26 **Ott et al. (2011)**). These techniques enable the derivation of low-dimensional dynamical systems that  
27 reveal the collective emergent behavior of the full discrete population (in the limit of an infinite number  
28 of interacting elements). In the context of computational neuroscience, these methods were applied to  
29 autonomous globally-coupled networks of canonical Type-I neurons (i.e., theta neurons) by **Luke et al.**

30 (2013), and to non-autonomous theta neuron networks by **So et al.** (2014). More recently, **Laing** (2014)  
 31 extended these results to include space-dependent coupling. A similar approach, based on phase-response  
 32 curves, was pursued by **Pazó and Montbrió** (2014).

33 Of course, such networks lack the intricate connectivity found in real biological networks. Neverthe-  
 34 less, they are ideal building blocks for the construction of a more realistic, yet mathematically tractable,  
 35 network-of-networks representation of the brain. In the current study, we consider the simplest hiera-  
 36 rchical structure as a first step in this process. Using two globally-coupled networks of theta neurons, we  
 37 arrange for the emergent collective activity of one population to drive the second population. Thus the ove-  
 38 rall network has an autonomous driver-response configuration. We demonstrate that even in this simplest  
 39 network-of-networks, the collective behavior of the response network can exhibit a full range of complex  
 40 behavior, from simple collective rhythms to temporally chaotic dynamics. Most importantly, we provide  
 41 a complete nonlinear dynamical analysis of this system, including predictive bifurcation diagrams for the  
 42 behavior of the response population in terms of the driver’s dynamics and the network characteristics.

## 2 RECAP OF SINGLE POPULATION RESULTS

### 2.1 THE THETA NEURON

43 Neurons are typically classified into two types, based on the nature of the onset of spiking as a con-  
 44 stant injected current exceeds an effective threshold (**Hodgkin** (1948); **Ermentrout** (1996); **Izhikevich**  
 45 (2007)). Type-I neurons begin to spike at an arbitrarily low rate, whereas Type-II neurons spike at a  
 46 non-zero rate as soon as the threshold is exceeded. Neurophysiologically, excitatory pyramidal neurons  
 47 are often of Type-I, and fast-spiking inhibitory interneurons are often of Type-II (**Nowak et al.** (2003);  
 48 **Tateno et al.** (2004)). Near the onset of spiking, Type-I neurons can be represented by a canonical phase  
 49 model that features a saddle-node bifurcation on an invariant cycle, or SNIC bifurcation (**Ermentrout**  
 50 **and Kopell** (1986); **Ermentrout** (1996)). This model has come to be known as the theta neuron, and is  
 51 given by

$$\dot{\theta} = (1 - \cos \theta) + (1 + \cos \theta)\eta, \quad (1)$$

52 where  $\theta$  is a phase variable on the unit circle and  $\eta$  is a bifurcation parameter related to the injected current.  
 53 For  $\eta < 0$ , the neuron is attracted to a stable equilibrium which represents the resting state. An unstable  
 54 equilibrium is also present, representing the threshold. If an external stimulus pushes the neuron’s phase  
 55 across the unstable equilibrium,  $\theta$  will move around the circle and approach the resting equilibrium from  
 56 the other side. When  $\theta$  crosses  $\theta = \pi$ , the neuron is said to have spiked. Thus, for  $\eta < 0$ , the neuron  
 57 is excitable. As the parameter  $\eta$  increases, these equilibria approach each other and merge via the SNIC  
 58 bifurcation at  $\eta = 0$ . At this point, the equilibria disappear, leaving a limit cycle. The neuron spikes  
 59 regularly for  $\eta > 0$ . In the following, we call  $\eta$  the “excitability parameter”.

### 2.2 A NETWORK OF THETA NEURONS

60 We formulate a single population of  $N$  theta neurons as follows:

$$\dot{\theta}_j = (1 - \cos \theta_j) + (1 + \cos \theta_j)[\eta_j + I_{syn}], \quad (2)$$

61 where  $j = 1, \dots, N$  is the index for the  $j$ -th neuron. The neurons are coupled via a pulse-like synaptic  
 62 current

$$I_{syn} = \frac{k}{N} \sum_{i=1}^N P_n(\theta_i), \quad (3)$$

63 where  $P_n(\theta) = a_n (1 - \cos \theta)^n$ ,  $n \in \mathbb{N}$ , and  $a_n$  is a normalization constant <sup>1</sup>

$$\int_0^{2\pi} P_n(\theta) d\theta = 2\pi.$$

64 The parameter  $n$  defines the sharpness of the pulse-like synapse in that  $P_n(\theta)$  becomes more and more  
65 sharply peaked as  $n$  increases. We assume that the synaptic strength  $k$  is the same for all neurons.

66 Note that the connectivity described by Eqs. (2) and (3) includes self-coupling terms. These have negli-  
67 gible effect on the collective network dynamics (data not shown), which is to be expected since they  
68 represent only one out of  $N$  inputs to any given neuron. Nevertheless, we note that these self-connections  
69 have real-world analogs in “autapses”, which have been found in several regions of the brain (e.g., **Bacci**  
70 **et al.** (2003); **Bekkers** (2003)).

71 Neurons in real biological networks exhibit a range of different intrinsic dynamics. We model this by  
72 taking the excitability parameter  $\eta_j$  of each neuron to be different, with each  $\eta_j$  being drawn randomly  
73 from a distribution  $g(\eta)$ . In the following analysis, we assume a Lorentzian distribution,

$$g(\eta) = \frac{1}{\pi} \frac{\Delta}{(\eta - \eta_0)^2 + \Delta^2}, \tag{4}$$

74 where  $\eta_0$  is the center of the distribution, and  $\Delta$ , the half-width at half-maximum, describes the degree of  
75 heterogeneity in the population.

### 2.3 REDUCTION AND ASYMPTOTIC STATES OF THE SINGLE POPULATION

76 The macroscopic behavior of our network can be quantified by the “macroscopic mean field”, or order  
77 parameter, defined as

$$\tilde{z}(t) = \sum_{j=1}^N e^{i\theta_j}, \tag{5}$$

78 where the tilde indicates that the sum is over a finite population of  $N$  oscillators. (Below we will drop the  
79 tilde in the case of an infinite network.) The magnitude of the order parameter  $|\tilde{z}(t)| \in [0, 1]$  quantifies the  
80 degree of synchronization present at time  $t$ .

81 In **Luke et al.** (2013), we used the Ott-Antonsen method (**Ott and Antonsen** (2008, 2009); **Ott et al.**  
82 (2011)) to derive a low-dimensional dynamical system whose asymptotic dynamics can be shown to  
83 coincide with that of the order parameter of the single-population network defined above (Eqs. (2)-(4)), in  
84 the limit  $N \rightarrow \infty$ . This reduced dynamical system is

$$\dot{z} = -i \frac{(z - 1)^2}{2} + \frac{(z + 1)^2}{2} \{-\Delta + i[\eta_0 + kH_n(z)]\}, \tag{6}$$

85 where

$$H_n(z) = I_{syn}/k = a_n \left( A_0 + \sum_{q=1}^n A_q (z^q + z^{*q}) \right), \tag{7}$$

86

$$A_q = \sum_{j,m=0}^n \delta_{j-2m,q} Q_{jm}, \tag{8}$$

---

<sup>1</sup>  $a_n = 2\pi / \int_{-\pi}^{\pi} (1 - \cos(x))^n = n! / (2n - 1)!!$

87 and

$$Q_{jm} = \frac{(-1)^{j-2m} n!}{2^j m! (n-j)! (j-m)!} \quad (9)$$

88 In these equations,  $z^*$  denotes the complex conjugate of  $z$ , and  $\delta_{i,j}$  is the Kronecker delta function on the  
89 indices  $(i, j)$ . Note that  $H_n(z) = H_n^*(z)$  is a real-valued function.

90 The analysis of Eqs. (6)-(9) reported in **Luke et al.** (2013) showed that the theta neuron network can  
91 exhibit three types of asymptotic states. These correspond to a node, a focus, and a limit cycle in the order  
92 parameter. A complete bifurcation analysis describing how these states change as the parameters  $k$ ,  $\eta_0$ ,  
93 and  $\Delta$  change was also reported. For our purposes in the current work, we now briefly describe the three  
94 possible collective macroscopic states.

95 We called the node, focus, and limit cycle solutions the ‘‘Partially Synchronous Rest’’ (PSR), ‘‘Partially  
96 Synchronous Spiking’’ (PSS), and ‘‘Collective Periodic Wave’’ (CPW) states, respectively. In the PSR  
97 state, most neurons remain at rest, while in the PSS state, most neurons spike continuously. Nevertheless,  
98 in both these states, the macroscopic mean field (or order parameter) sits at an equilibrium. In contrast,  
99 the CPW state corresponds to periodic oscillations of the complex order parameter, and typically, both  
100  $|z(t)|$  and  $\arg(z)$  oscillate in time indicating that the individual neurons clump together and spread apart  
101 in a periodic fashion. We refer the interested reader to **Luke et al.** (2013) for further details, including  
102 movies that illustrate both the microscopic and macroscopic behaviors of these collective states.

### 3 FORMULATION OF THE DRIVER-RESPONSE NETWORK

103 In this work, we are interested in the dynamics exhibited by a network of two coupled populations of  
104 theta neurons. We formulate the general case, but restrict analysis to the simplest such configuration: a  
105 driver-response network.

#### 3.1 GENERAL TWO-POPULATION MODEL

Extending the model described above, a general formulation of pair of interacting populations of theta  
neurons can be expressed as follows:

$$\begin{aligned} \dot{\theta}_{1,j} &= 1 + \eta_{1,j} - (1 - \eta_{1,j}) \cos \theta_{1,j} \\ &+ a_n (1 + \cos \theta_{1,j}) \left[ \frac{k_{11}}{N_1} \sum_{p=1}^{N_1} (1 - \cos \theta_{1,p})^n + \frac{k_{12}}{N_2} \sum_{q=1}^{N_2} (1 - \cos \theta_{2,q})^n \right], \\ \dot{\theta}_{2,j} &= 1 + \eta_{2,j} - (1 - \eta_{2,j}) \cos \theta_{2,j} \\ &+ a_n (1 + \cos \theta_{2,j}) \left[ \frac{k_{21}}{N_1} \sum_{p=1}^{N_1} (1 - \cos \theta_{1,p})^n + \frac{k_{22}}{N_2} \sum_{q=1}^{N_2} (1 - \cos \theta_{2,q})^n \right], \end{aligned} \quad (10)$$

106 where  $\theta_{1,j}$  and  $\theta_{2,j}$  denote the  $j$ th neuron in the first and second populations, respectively, and the exten-  
107 sion to any number of interacting populations is straightforward. The excitability parameters  $\eta_{1,j}$  and  $\eta_{2,j}$   
108 are randomly drawn from independent Lorentzian distributions as in Eq. (4), with medians  $\eta_1$ ,  $\eta_2$  and  
109 widths  $\Delta_1$ ,  $\Delta_2$ , respectively. We take the sharpness parameter of the pulse-like synaptic interaction,  $n$ , to  
110 be the same for both populations. Macroscopic mean field parameters  $\tilde{z}_1(t)$ ,  $\tilde{z}_2(t)$  can be defined for each  
111 population by analogy with Eq. (5).

112 Adapting the procedures described in **Luke et al.** (2013), we derived the Ott-Antonsen reduction of the  
113 coupled networks of Eq. (10). This resulted in the following dynamical system:

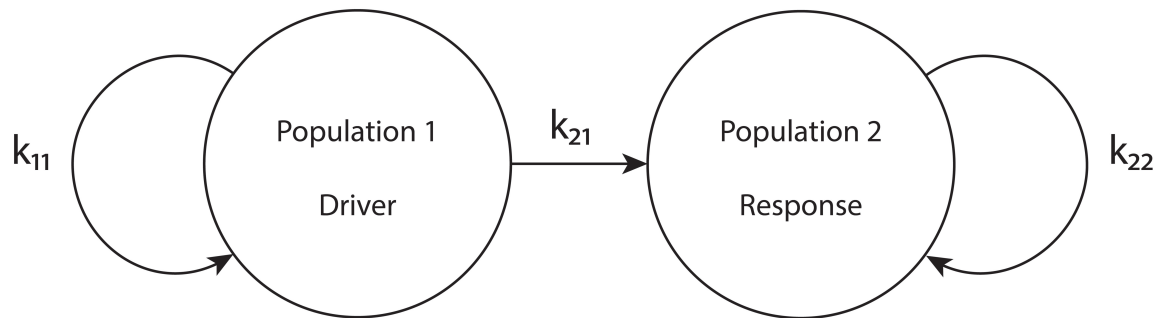


**Figure 1.** The driver-response configuration.  $k_{11}$  and  $k_{22}$  are the intra-population coupling strengths for populations 1 and 2, respectively, and  $k_{21}$  is the uni-directional coupling strength between the driver population (1) and the response population (2).

$$\begin{aligned} \dot{z}_1 &= -i\frac{(z_1 - 1)^2}{2} + \frac{(z_1 + 1)^2}{2} \{-\Delta_1 + i[\eta_1 + k_{11}H_n(z_1) + k_{12}H_n(z_2)]\}, \\ \dot{z}_2 &= -i\frac{(z_2 - 1)^2}{2} + \frac{(z_2 + 1)^2}{2} \{-\Delta_2 + i[\eta_2 + k_{21}H_n(z_1) + k_{22}H_n(z_2)]\}. \end{aligned} \quad (11)$$

114 with  $H_n(z)$  defined as in Eqs. (7)-(9). As before, the asymptotic dynamics of Eqs. (11) can be shown  
 115 to coincide with that of the order parameters of the populations in the network of Eq. (10), in the limit  
 116  $N_1, N_2 \rightarrow \infty$ .

117 We showed in **Luke et al. (2013)** that the dynamical structure of the single population depends rather  
 118 weakly on the synaptic sharpness parameter  $n$ . Furthermore, we argued that a modest sharpness is more  
 119 biophysically plausible than the  $\delta$ -function coupling obtained in the limit  $n \rightarrow \infty$ . Thus, from here on,  
 120 we fix  $n = 2$  and drop the subscript on  $H_n$  to ease notation.

### 3.2 THE DRIVER-RESPONSE SYSTEM

121 To put our network in driver-response form, we set  $k_{12} = 0$ , so that population 1 receives no input from  
 122 population 2. Therefore, the macrostates and bifurcations of population 1 are identical to those explored in  
 123 **Luke et al. (2013)**, described above. However, we allow  $k_{21} \neq 0$ . Our goal is to examine the consequences  
 124 of the influence of population 1 on population 2. We call population 1 the “driver” and population 2 the  
 125 “response” system. See Figure 1.

126 Writing the governing equation of population 2 as

$$\dot{z}_2 = -i\frac{(z_2 - 1)^2}{2} + \frac{(z_2 + 1)^2}{2} \{-\Delta_2 + i[\eta_{eff} + k_{22}H(z_2)]\} \quad (12)$$

127 with

$$\eta_{eff} \equiv \eta_2 + k_{21}H(z_1), \quad (13)$$

128 and comparing to Eq. (6), we see that the behavior of population 2 is the same as that of a single population  
 129 of theta neurons with an effective median excitability parameter  $\eta_{eff}$ . This effective parameter depends  
 130 on  $\eta_2$ , the median excitability parameter intrinsic to population 2, the inter-population coupling  $k_{21}$ , and  
 131 the state of the driver  $z_1$ .

132 Note that  $\eta_{eff}$  depends linearly on both  $\eta_2$  and  $k_{21}$  and nonlinearly on the driver's state  $z_1$  through  
 133  $H(z_1)$ . Additionally,  $\eta_{eff}$  may be time-dependent if population 1 exhibits a CPW state, since in that case  
 134  $z_1$  oscillates periodically. In the following, we will examine all these cases.

## 4 RESULTS

135 We will examine the behavior of population 2 as various parameters are varied. We organize the presen-  
 136 tation of our results by first considering the case in which the driver population exhibits an equilibrium  
 137 state. Later, we consider the case in which the driver population exhibits periodic behavior.

138 We will mainly consider two configurations of the response system. The “excitatorily coupled” response  
 139 system has  $k_{22} > 0$ , and the “inhibitorily coupled” response system has  $k_{22} < 0$ . Other parameters are as  
 140 noted below.

141 The bifurcation diagrams that appear below in Figures 2, 3, 4B, 5B, and 8C were obtained using  
 142 XPPAUT (Ermentrout (2002)). Data for all other figures were generated using custom-designed code.

### 4.1 DRIVER ON A MACROSCOPIC EQUILIBRIUM

143 We begin by fixing the driving population's parameters at  $\eta_1 = -0.2$ ,  $\Delta_1 = 0.1$ , and  $k_{11} = -2$ , which  
 144 corresponds to a PSR state. Thus  $z_1$  remains fixed at a constant value. We examine the behavior of the two  
 145 response system configurations as we vary the inter-population coupling parameter,  $k_{21}$ . From Eq. (13),  
 146  $\eta_{eff}$  varies linearly with respect to  $k_{21}$ .

147 *4.1.1 Excitatorily-coupled response system* We set the response system's internal coupling to  $k_{22} = 9$ ,  
 148 and show in Figure 2A the two-parameter bifurcation diagram of the response system with respect to  $\Delta_2$   
 149 and  $\eta_{eff}$ . Two saddle-node bifurcation curves which meet at a cusp are seen. To the left of these curves,  
 150 the response network exhibits a PSR state, and to the right, a PSS state. These states coexist inside the  
 151 approximately triangular region.

152 We set the remaining parameters of the response system to  $\eta_2 = -10$  and  $\Delta_2 = 0.5$ . Thus, for  $k_{21} = 0$ ,  
 153  $\eta_{eff} = \eta_2$ , and the response system is situated at the solid black point marked in Figure 2A. As  $k_{21}$   
 154 increases from zero,  $\eta_{eff}$  increases linearly along the dotted line in Figure 2A, starting from the black  
 155 point. In so doing, it traverses the SN bifurcation curves. Figure 2B shows how the imaginary part of the  
 156 response's asymptotic macroscopic mean field ( $y_2 = \text{Im}(z_2)$ ) changes with respect to  $k_{21}$ , illustrating the  
 157 coexistence of the stable PSR and PSS states, along with an unstable PSR state (uPSR).

158 The point marked “SN/NF” in Figure 2B indicates that as  $k_{21}$  increases, a saddle node bifurcation is  
 159 encountered, corresponding to the left SN curve in Figure 2A. This creates a stable and an unstable PSS  
 160 state. However, the unstable PSS state converts into an unstable PSR state at a value of  $k_{21}$  very slightly  
 161 beyond the SN bifurcation. That is, the node corresponding to the unstable PSS state becomes a unstable  
 162 PSR focus, a transition we called a Node-Focus (NF) transition in Luke et al. (2013). The distinction  
 163 between these events is indistinguishable in the figure.

164 *4.1.2 Inhibitorily-coupled response system* We performed a similar analysis for the case in which the  
 165 response system's internal coupling is  $k_{22} = -9$ , i.e., inhibitory, and  $\eta_2 = 5$ . The remaining parameters  
 166 were unchanged. The results are shown in Figure 3. In this case, the two-dimensional bifurcation diagram  
 167 of the response system with respect to  $\Delta_2$  and  $\eta_{eff}$  (Figure 3A) shows a similar (but mirror-image)  
 168 cusp of saddle-node curves. A new feature is the occurrence of a codimension-2 Bogdanov-Takens (BT)  
 169 point on the left SN curve, and the emergence of homoclinic (HC; green) and Andronov-Hopf (AH; red)  
 170 bifurcation curves from the BT point.

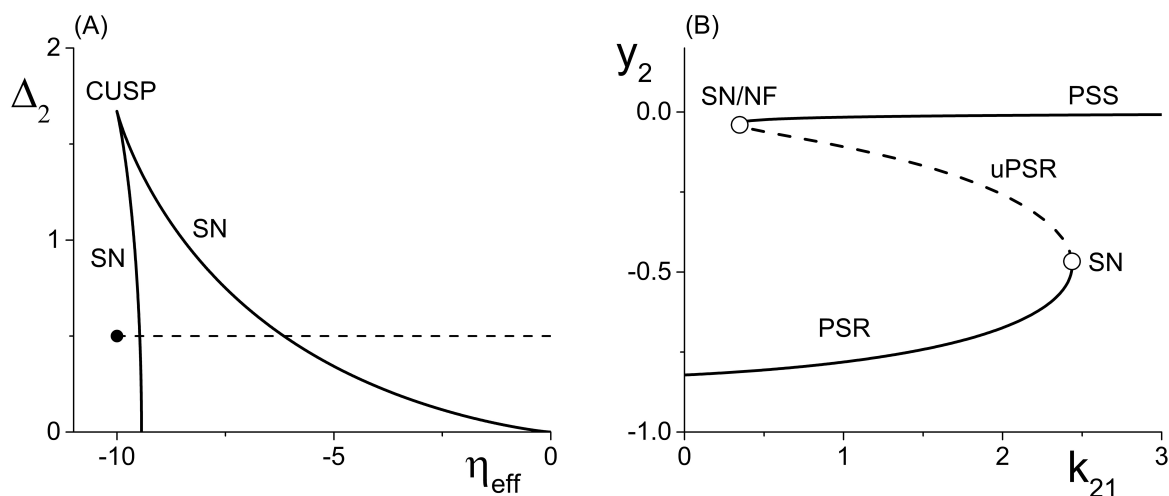


**Figure 2.** (A) A two-dimensional bifurcation diagram of the excitatorily-coupled response system. The heavy black lines are saddle-node (SN) bifurcation curves, and the solid dot denotes the parameters of the response system when decoupled from the driver. In the cases considered in the main text, the driver causes  $\eta_{eff}$  to vary along the horizontal dotted line. The parameters are:  $\eta_1 = -0.2$ ,  $\Delta_1 = 0.1$ ,  $k_{11} = -2$ , and  $k_{22} = 9$ . (B) The one-dimensional bifurcation diagram showing the asymptotic values of  $y_2 = \text{Im}(z_2)$  vs.  $k_{21}$ . Solid and dashed curves indicate stable and unstable equilibria, respectively, corresponding to partially synchronous spiking (PSS) and partially synchronous resting (PSR) states. The parameters are as in panel (A), with  $\eta_2 = -10$  and  $\Delta_2 = 0.5$ .

171 Figure 3B shows how the real part of the response’s asymptotic macroscopic mean field ( $x_2 = \text{Re}(z_2)$ )  
 172 changes with respect to  $k_{21}$ . As before,  $\eta_{eff}$  increases linearly as  $k_{21}$  increases, starting from the black  
 173 solid point in Figure 3A and moving toward the right, traversing the various bifurcation curves along the  
 174 dotted line. Note the presence of the attracting limit cycle CPW state in Figure 3B, which emerges at the  
 175 HC bifurcation and terminates at the AH bifurcation as  $k_{21}$  increases.

176 It is interesting to note that in both cases described above, the same bifurcation structure would be  
 177 encountered if, instead of varying  $k_{21}$  with a fixed value  $\eta_2$ , we varied  $\eta_2$  with a fixed value of  $k_{21}$ .  
 178 While this is obvious from Eq. (13) since  $H(z_1)$  is constant in these cases, this leads to the non-obvious  
 179 conclusion that by modifying either the inter-population coupling or the intrinsic median excitability of  
 180 the response population — two rather different system characteristics — one obtains identical transitions  
 181 in the response network.

182 **4.1.3 Variation of the driver’s macroscopic equilibrium** In the cases we considered previously,  $\eta_{eff}$   
 183 changed linearly with respect to the inter-population coupling  $k_{21}$ . We now turn our attention to the effects  
 184 incurred by altering the value of the driver influence function  $H(z_1)$  in Eq. (13). We do this by varying the  
 185 driver’s internal coupling strength  $k_{11}$ , thus causing the driver’s asymptotic macroscopic mean field  $z_1$  to  
 186 change. This manipulation has the effect of changing  $\eta_{eff}$  *nonlinearly* with respect to  $k_{11}$ .

187 For simplicity, we only consider a range of  $k_{11}$  such that the driver always remains on a macroscopic  
 188 equilibrium state, and we fix the inter-population coupling at  $k_{21} = 2.0$ .

189 We begin with the case of the excitatorily-coupled response system considered above, with  $\eta_2 = -10$ ,  
 190  $\Delta_2 = 0.5$ , and  $k_{22} = 9$ , and choose the remaining driver parameters to be  $\eta_1 = -0.05$  and  $\Delta_1 = 0.05$ .  
 191 Figure 4A shows the nonlinear behavior of  $\eta_{eff}$  as  $k_{11}$  is varied. Even though we are considering  $k_{11}$   
 192 to be the independent parameter, we plot  $\eta_{eff}$  horizontally so that it may be easily compared to Figure

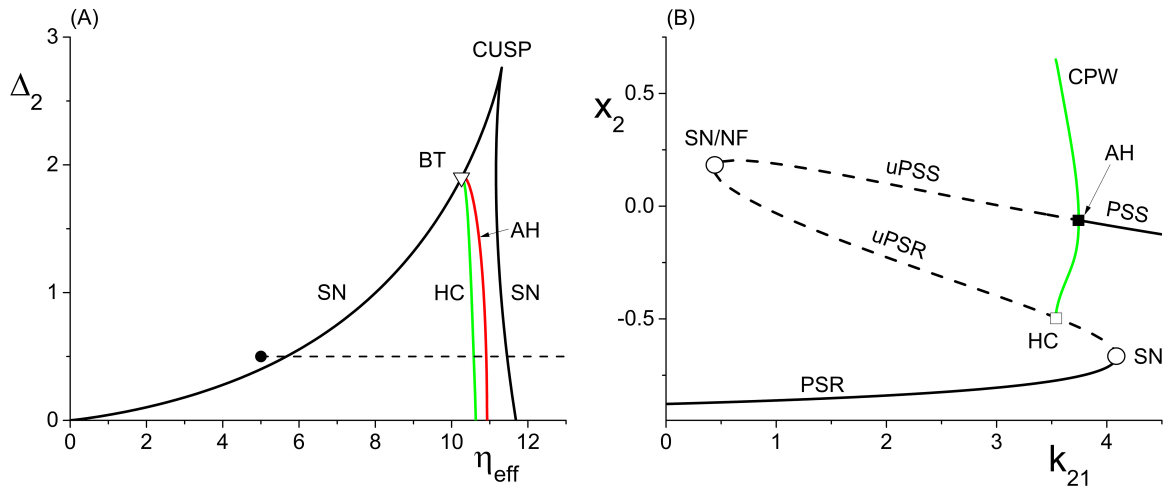


**Figure 3.** (A) The two-dimensional bifurcation diagram of the inhibitorily-coupled response system. The heavy black lines are saddle-node (SN) bifurcation curves, green is a homoclinic (HC) bifurcation curve, and red is an Andronov-Hopf (AH) bifurcation curve. The latter two curves emerge from a Bogdanov-Takens (BT) point. The solid dot denotes the parameters of the response system when decoupled from the driver. In the cases considered in the main text, the driver causes  $\eta_{eff}$  to vary along the horizontal dotted line. The parameters are:  $\eta_1 = -0.2$ ,  $\Delta_1 = 0.1$ ,  $k_{11} = -2$ , and  $k_{22} = -9$ . (B) The one-dimensional bifurcation diagram showing the asymptotic value of  $x_2 = \text{Re}(z_2)$  vs.  $k_{21}$ . Solid curves denote stable equilibria; dashed black curves are unstable equilibria. Green represents the maxima and minima of a collective periodic wave (CPW) limit cycle. The parameters are as in panel (A), with  $\eta_2 = 5$  and  $\Delta_2 = 0.5$ .

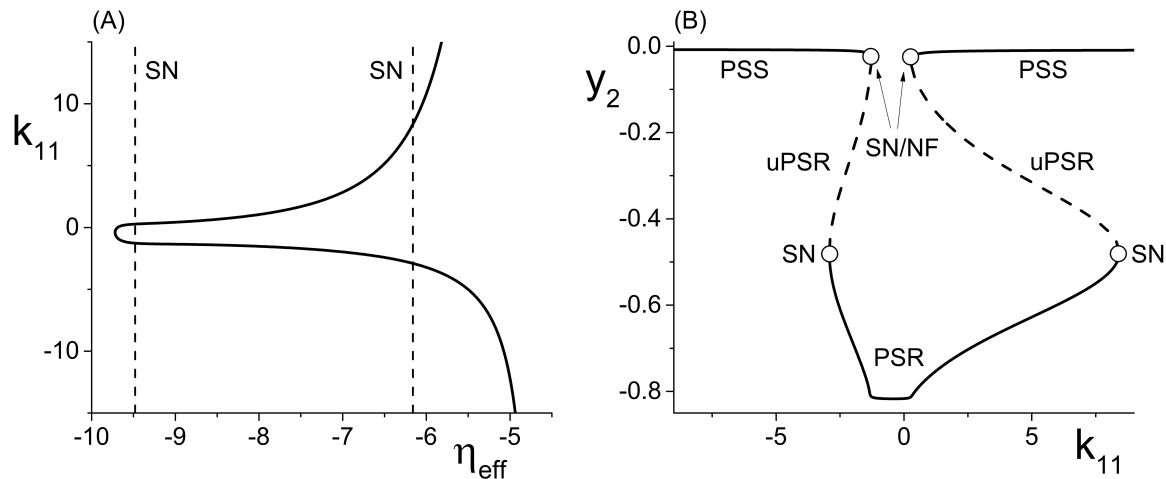


**Figure 4.** (A) The nonlinear behavior of  $\eta_{eff}$  as a function of  $k_{11}$  for the excitatorily-coupled response system.  $\eta_{eff}$  is plotted horizontally to facilitate comparison with Figure 2A. The parameters are:  $\eta_1 = -0.05$ ,  $\Delta_1 = 0.05$ ,  $\eta_2 = -10$ , with the inter-population coupling fixed at  $k_{21} = 2.0$ . (B) The one-dimensional bifurcation diagram showing the asymptotic value of  $y_2 = \text{Im}(z_2)$  vs.  $k_{11}$ . Solid and dashed curves indicate stable and unstable equilibria, respectively. The parameters are as in panel (A), with  $\Delta_2 = 0.5$  and  $k_{22} = 9$ .

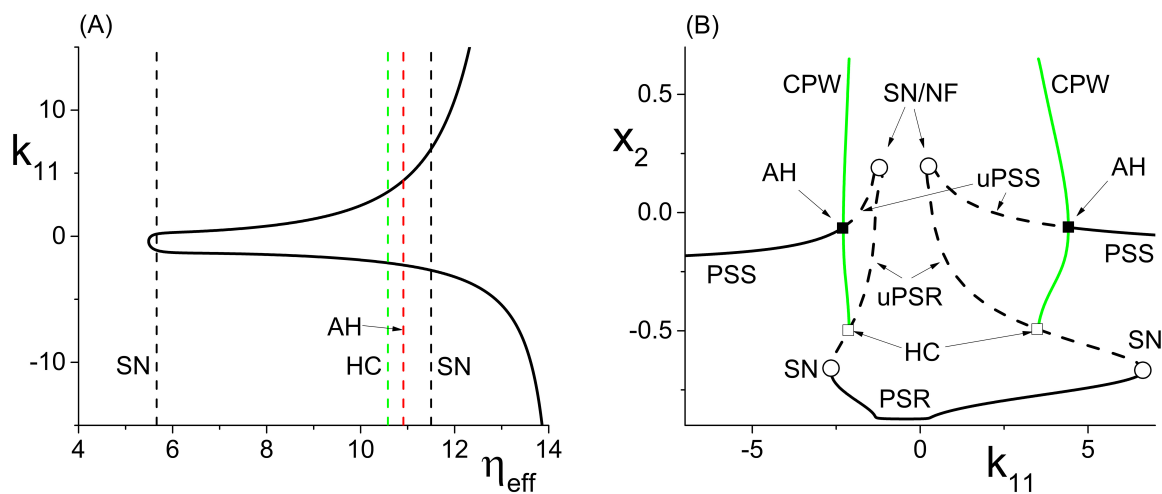


**Figure 5.** (A) The nonlinear behavior of  $\eta_{eff}$  as a function of  $k_{11}$  for the inhibitorily-coupled response system.  $\eta_{eff}$  is plotted horizontally to facilitate comparison with Figure 3A. (B) The one-dimensional bifurcation diagram showing the asymptotic value of  $x_2 = \text{Im}(z_2)$  vs.  $k_{11}$ . Solid and dashed black curves indicate stable and unstable equilibria, respectively, and green represents the maxima and minima of a CPW limit cycle state. The parameters are:  $\eta_1 = -0.05$ ,  $\Delta_1 = 0.05$ ,  $\eta_2 = 5$ ,  $\Delta_2 = 0.5$ , and  $k_{22} = -9$ . The inter-population coupling is fixed at  $k_{21} = 3.5$ .

193 2A; recall that this shows the two-dimensional bifurcation diagram of the response system. Now, as  $k_{11}$   
 194 changes,  $\eta_{eff}$  moves back and forth along the dotted line nonlinearly. In particular, Figure 4A shows  
 195 that for very negative values of  $k_{11}$ ,  $\eta_{eff}$  is near  $-5$ , which corresponds to a point in Figure 2A to the  
 196 right of the SN curves. As  $k_{11}$  increases,  $\eta_{eff}$  decreases to approximately  $-10$ , thus crossing both SN  
 197 curves in Figure 2A from right to left in the process.  $\eta_{eff}$  subsequently increases, and goes back across  
 198 the SN curves from left to right. Note that Figure 4A includes vertical lines marking the position of the  
 199 SN bifurcations (i.e., the values of  $\eta_{eff}$  at which the horizontal line at  $\Delta_2 = 0.5$  in Figure 2A crosses the  
 200 SN curves).

201 Figure 4B shows the behavior of the asymptotic state of the response system ( $y_2 = \text{Im}(z_2)$ ) as a function  
 202 of  $k_{11}$ . This shows that as  $k_{11}$  increases, the response system passes through two separate regions of  
 203 bistability, corresponding to the two traversals of the triangular bistable region in Figure 2A. Thus Figure  
 204 4B is qualitatively similar to two copies of Figure 2B, with the structure for  $k_{11} < 0$  reversed. Note that  
 205 the two regions are not symmetrical. This is due to the nonsymmetric behavior of  $\eta_{eff}$  as  $k_{11}$  changes.

206 Next, we examine how the same manipulation of the driver system affects the inhibitorily-coupled  
 207 response system. The parameters are as above, but with  $\eta_2 = 5$  and  $k_{22} = -9$ . Figure 5A shows how  $\eta_{eff}$   
 208 changes as  $k_{11}$  is varied, again plotted with  $\eta_{eff}$  on the horizontal axis for ease of comparison with Figure  
 209 3A. Note the vertical lines in Figure 5A marking the SN, HC, and AH bifurcations.

210 The one-dimensional bifurcation diagram depicting the asymptotic state of the response system as a  
 211 function of  $k_{11}$  is shown in Figure 5B. A situation similar to the previous case is observed. Two distorted  
 212 versions of the structure of Figure 3B, with the features for  $k_{11} < 0$  being reversed, are seen. Again, this  
 213 is due to the nonlinear and asymmetric behavior of  $\eta_{eff}$  as it traverses the bifurcations in Figure 3A twice:  
 214 first right to left, and then left to right, as  $k_{11}$  is increased. Note also the presence of an attracting limit  
 215 cycle CPW state in intervals of both positive and negative  $k_{11}$ .

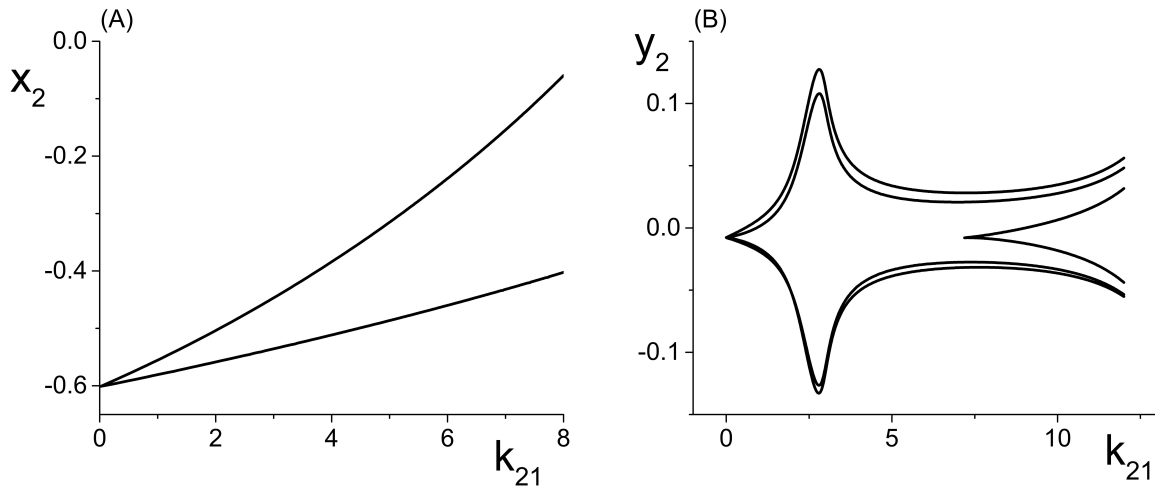


**Figure 6.** (A) Simple periodic behavior in the response system driven by a CPW state of the driver as a function of the inter-population coupling strength  $k_{21}$ . The curves are local maxima and minima of  $x_2 = \text{Re}(z_2)$ . The driver parameters are  $\eta_1 = 10.75$ ,  $\Delta_1 = 0.5$ , and  $k_{11} = -9$ , and the response parameters are  $\eta_2 = -20$ ,  $\Delta_2 = 0.5$ , and  $k_{22} = 9$ . (B) Slightly more complicated periodic behavior obtained at the same parameters, except with  $\eta_2 = -5$ . The curves are local maxima and minima of  $y_2 = \text{Im}(z_2)$ .

## 4.2 DRIVER ON A MACROSCOPIC LIMIT CYCLE

216 We now focus on the behavior of the response population when the driver is on a CPW state, which is a  
 217 limit cycle of the driver’s macroscopic mean field (or order parameter). Throughout this section, we fix the  
 218 driver parameters at  $\eta_1 = 10.75$ ,  $k_{11} = -9$ , and  $\Delta_1 = 0.5$ , which results in a CPW driver state for which  
 219  $H(z_1)$  oscillates periodically in time. In particular, we have  $H(z_1) > 0$  for all time. Thus, according to  
 220 Eq. (13),  $\eta_{eff}$  also oscillates periodically for  $k_{21} \neq 0$ , and both the centroid and the amplitude of the  $\eta_{eff}$   
 221 oscillation increase as  $k_{21}$  increases.

222 We show below that in this configuration, the response population can exhibit periodic, multista-  
 223 ble, chaotic, and/or quasiperiodic behavior, depending on the response system’s parameters and the  
 224 interpopulation coupling strength  $k_{21}$ .

225 *4.2.1 Periodic behavior in the response system* We begin by considering the excitatorily coupled  
 226 response system, with  $\Delta_2 = 0.5$  and  $k_{22} = 9$ , but with  $\eta_2 = -20$ . When decoupled from the driver,  
 227 this places the response system at a point well to the left in the parameter space of Figure 2A. Thus the  
 228 response system in isolation asymptotes to a PSR state. As  $k_{21}$  is increased from zero to eight,  $\eta_{eff}$  oscil-  
 229 lates back and forth along the horizontal line in Figure 2A at  $\Delta_2 = 0.5$ , but always stays to the left of  
 230 the SN curves shown in that figure. Thus, the driver simply pushes the response system’s PSR state back  
 231 and forth, avoiding any bifurcations. The result is simple periodic behavior in the driven response system.  
 232 Figure 6A shows a plot of the maximum and minimum of  $x_2 = \text{Re}(z_2)$  versus  $k_{21}$ . As  $k_{21}$  increases,  
 233 the amplitude of this simple periodic behavior increases. We observe that the frequency of the response  
 234 system’s oscillation is the same as that of the driver throughout this range of interpopulation coupling.

235 We now change the response system such that  $\eta_2 = -5$ , and leave all other parameters the same as  
 236 above. This change places the response system at a point to the right of the SN curves in Figure 2A,  
 237 and for these parameters, the uncoupled response system asymptotes to a PSS state. Once again, as  $k_{21}$

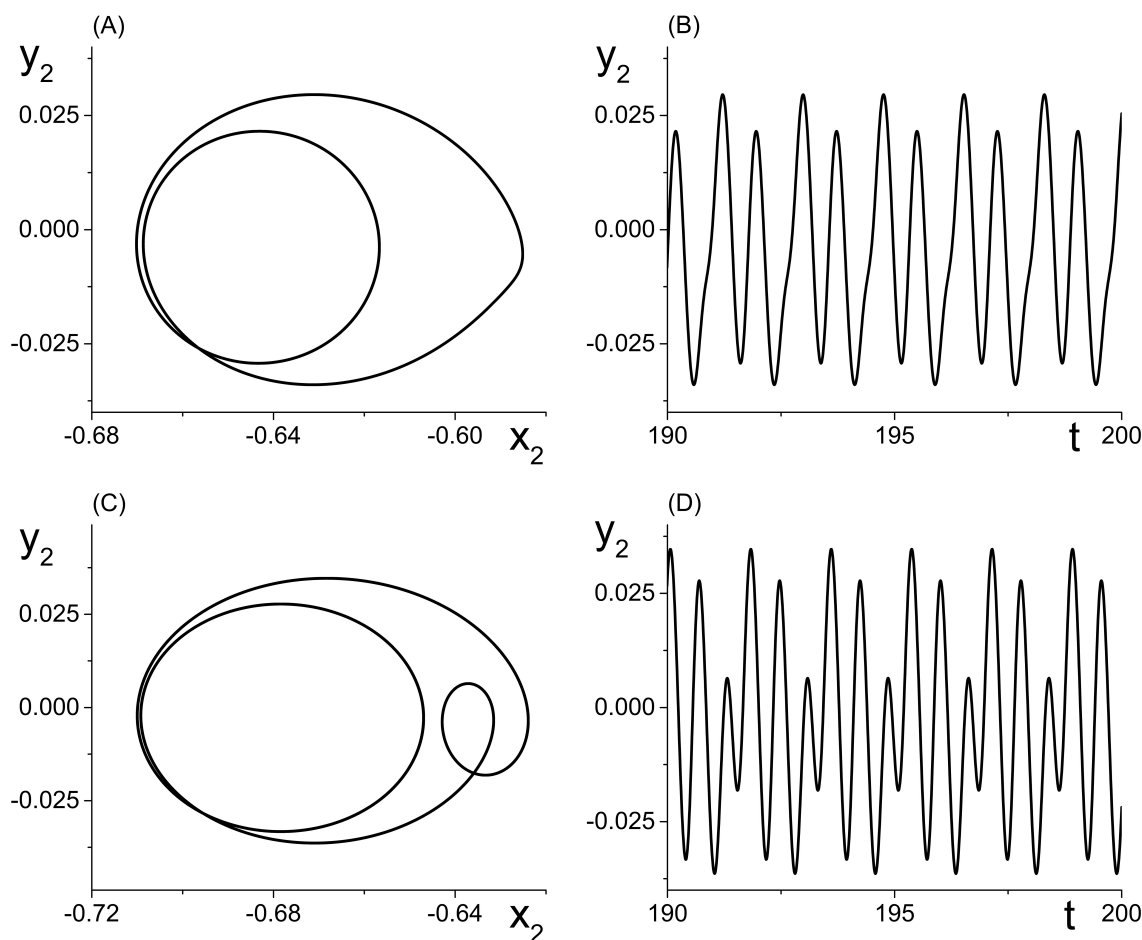


**Figure 7.** The response system’s behavior at parameters corresponding to Figure 6B at  $k_{21} = 6$  (A, B) and  $k_{21} = 10$  (C, D), with  $z_2 = x_2 + iy_2$ .

238 increases,  $\eta_{eff}$  oscillates back and forth along the  $\Delta_2 = 0.5$  line in Figure 2A, but this time it does so  
 239 always staying to the right of the SN curves.

240 The result is multi-frequency periodic behavior in the response system that is more complicated than in  
 241 the previous example. Figure 6B shows a plot of the *local* minima and maxima of  $y_2 = \text{Im}(z_2)$  versus  $k_{21}$ .  
 242 Figure 7 shows  $y_2$  vs.  $x_2$  plots of the periodic orbits at  $k_{21} = 6$  (upper panels) and  $k_{21} = 10$  (lower panels).  
 243 As  $k_{21}$  increases from zero, a periodic orbit with winding number two emerges (similar to that shown in  
 244 Figure 7A) and grows in amplitude, peaking near  $k_{21} \approx 2.5$ . The amplitude subsequently decreases to  
 245 a minimum near  $k_{21} \approx 7.2$ , and then slowly increases again. Note that the four curves in Figure 6B for  
 246  $k_{21} \in [0, 7.2]$  correspond to two pairs of alternating local maxima and minima in the time series of  $y_2$ , as  
 247 shown in Figure 7B.

248 Interestingly, near  $k_{21} \approx 7.2$ , an additional loop appears in the orbit, as shown in Figure 7C. This is  
 249 reflected in the additional inner curves in Figure 6B that appear for  $k_{21} \gtrsim 7.2$ , and the two additional local  
 250 maxima and minima in the time series of  $y_2$  in Figure 7D.

251 **4.2.2 Multistability in the response system** Continuing with the excitatorily coupled response system  
 252 (with  $k_{22} = 9 > 0$ ), we set  $\eta_2 = -10$  and leave all other parameters unchanged. In this case the uncoupled

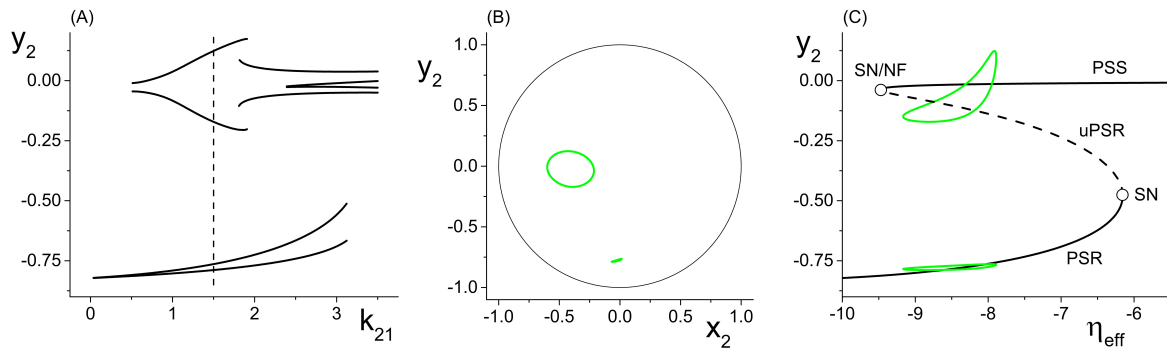


**Figure 8.** Multistability in the response system driven by a CPW state of the driver. (A) Local maxima and minima of  $y_2 = \text{Re}(z_2)$  vs. the inter-population coupling  $k_{21}$ . (B)  $y_2$  vs.  $x_2$  plots showing two coexisting limit cycles of the response system at  $k_{21} = 1.5$  (dotted vertical line in panel (A)). (C) The solid and dashed black curves show the asymptotic states of the response for fixed values of  $\eta_{eff}$ , with  $k_{21} = 1.5$ . Green curves are coexisting limit cycles of the response system when coupled to the driver. Parameters are:  $\eta_1 = 10.75$ ,  $\Delta_1 = 0.5$ ,  $k_{11} = -9$ ;  $\eta_2 = -10$ ,  $\Delta_2 = 0.5$ ,  $k_{22} = 9$ .

253 response system is at a point just to the left of the left SN curve in Figure 2A, and as  $k_{21}$  increases,  
 254  $\eta_{eff}$  again sweeps back and forth along the horizontal line at  $\Delta_1 = 0.5$ . However, now this sweeping  
 255 cuts across both SN curves. Thus, the response system sweeps back and forth across the approximately  
 256 triangular multistable region bounded by the SN curves.

257 Figure 8A shows the maxima and minima of  $x_2$  vs.  $k_{21}$  for this case. The first feature to emerge as  $k_{21}$   
 258 increases from zero is a simple periodic orbit whose amplitude increases, similar to the example in Figure  
 259 6A. At  $k_{21} \approx 0.5$ , a new and separate coexisting limit cycle appears, as indicated by the upper curves that  
 260 emerge in Figure 8A. Figure 8B shows the  $y_2$  vs.  $x_2$  plots of these two limit cycles at  $k_{21} = 1.5$ , where  
 261 the larger orbit corresponds to the upper two curves in Figure 8A. In this bistable region, the macroscopic  
 262 dynamics of the response system approaches one or the other of these periodic states, depending on the  
 263 initial conditions.

264 Figure 8C shows, in black, the asymptotic states of  $y_2$  vs.  $\eta_{eff}$  for *fixed* values of  $\eta_{eff}$ , with  $k_{21} = 1.5$ .  
 265 These curves show that for a large interval of  $\eta_{eff}$ , a stable PSR coexists with a stable PSS and an  
 266 unstable PSR state for the frozen (i.e.,  $\eta_{eff}$  fixed) system. With the driver on the CPW state,  $\eta_{eff}$  sweeps  
 267 from approximately  $-9.1$  to  $-7.6$  and back again – a range which is well within the bistable region.  
 268 Superimposed in green in Figure 8C are projections of the two coexisting limit cycles onto this space,  
 269 showing that the lower limit cycle is a simple periodic perturbation of the response system’s underlying  
 270 PSR state, and the upper limit cycle is a periodic perturbation of the underlying PSS state.

271 **4.2.3 Chaos in the response system** We now switch to the inhibitorily coupled response system, with  
 272 parameters  $\eta_2 = 5$ ,  $\Delta_2 = 0.5$ , and  $k_{22} = -9$ . The parameter space of this system is shown in Figure  
 273 3A, and the uncoupled response system resides at the solid black dot in that figure, to the left of all  
 274 the bifurcations. As the interpopulation coupling strength  $k_{21}$  increases,  $\eta_{eff}$  sweeps across the same  
 275 horizontal line at  $\Delta_2 = 0.5$  with increasing amplitude and centroid, initially crossing just the left SN  
 276 bifurcation curve. At  $k_{21} \approx 5.2$ ,  $\eta_{eff}$  begins sweeping across the homoclinic and the Andronov-Hopf  
 277 bifurcation curves. Eventually, for sufficiently large  $k_{21}$ ,  $\eta_{eff}$  sweeps across all four bifurcation curves  
 278 (SN, AH, HC, and SN).

279 Figure 9A shows the local maxima and minima of  $x_2 = \text{Re}(z_2)$  vs.  $k_{21}$ . We initially see the emergence  
 280 of a simple periodic orbit that grows slowly in amplitude. However, at  $k_{21} \approx 5.2$ , chaos suddenly emerges

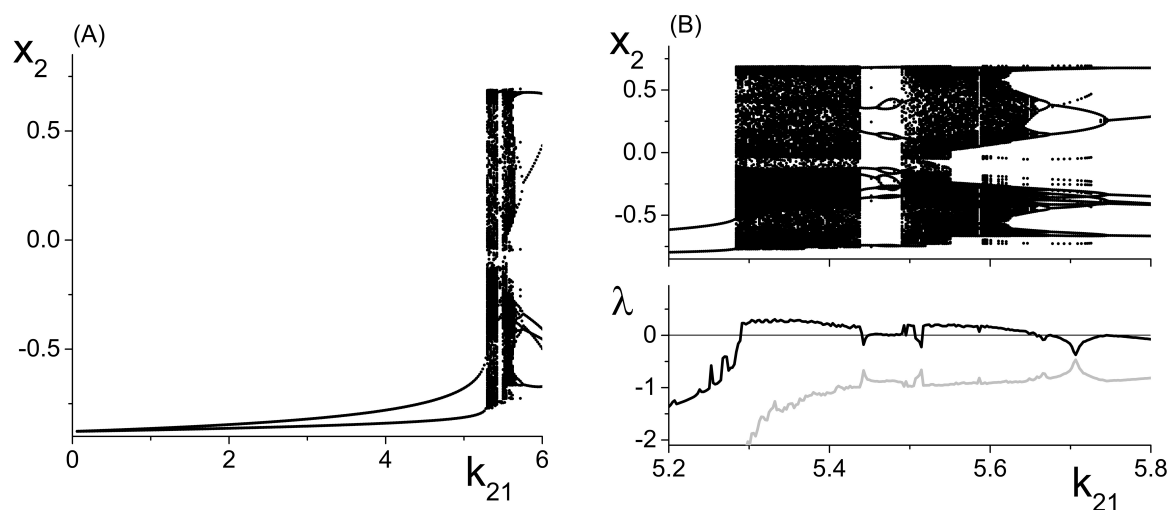


**Figure 9.** Emergence of macroscopic chaos in the response system driven by a CPW state of the driver. (A) Local minima and maxima of  $x_2 = \text{Re}(z_2)$  vs. the inter-population coupling  $k_{21}$ . (B) Magnification of the chaotic region (top), with a plot of the largest two Lyapunov exponents. Parameters are:  $\Delta_1 = 0.5$ ,  $k_{11} = -9$ ,  $\eta_1 = 10.75$ ;  $\Delta_2 = 0.5$ ,  $k_{22} = -9$ ,  $\eta_2 = 5$ .

281 through a crisis. Figure 9B shows a magnification of this region, with a plot of the two largest Lyapu-  
 282 nov exponents. We see that there are significant intervals of  $k_{21}$  for which there is a positive Lyapunov  
 283 exponent, indicating the presence of macroscopic chaos.

284 As  $k_{21}$  increases, the first chaotic band, beginning at  $k_{21} \approx 5.28$ , coexists with the simple periodic  
 285 loop that was present for smaller  $k_{21}$  (this coexistence is not apparent in the figure). Outside of this band,  
 286 there is a window dominated by periodic behavior of rather high period. A second chaotic band appears at  
 287 approximately  $k_{21} = 5.48$ . This second band terminates at approximately  $k_{21} = 5.65$ , after which a series  
 288 of reverse period-doubling cascades are seen.

289 The  $y_2$  vs.  $x_2$  plot of the chaotic attractor present at  $k_{21} = 5.296$ , for which the largest Lyapunov  
 290 exponent is approximately 0.2118, is shown in Figure 10A.

291 **4.2.4 Quasiperiodicity in the response system** Finally, we consider the case in which the response  
 292 system exhibits a CPW state when uncoupled from the driver, and ask what happens when this is driven by  
 293 another CPW state in the driver. We use the same drive system parameters as above, and set the response  
 294 system's parameters to be the same except for  $\Delta_2 = 0.3$ . As the inter-population coupling strength  $k_{21}$  is  
 295 increased, various phase-locked and quasiperiodic states are seen. An example of quasiperiodic behavior  
 296 in the response system for  $k_{21} = 0.1$  is shown in Figure 10B.

## 5 DISCUSSION

297 In this work, we have taken the first step towards designing a mathematically tractable modular network-  
 298 of-networks representation of neuronal systems. Our approach is based on dynamical analysis techniques  
 299 that enable a complete description of the emergent macroscopic behavior of large, heterogeneous discrete  
 300 networks of globally-coupled phase oscillators. Building on previous results (Luke et al. (2013)) in which  
 301 we used these techniques to show that the collective dynamics of a single such population of theta neurons  
 302 is relatively simple (exhibiting just equilibria and limit cycle states), we constructed the next simplest  
 303 hierarchical structure: a driver-response configuration of theta neuron populations. Our results show that

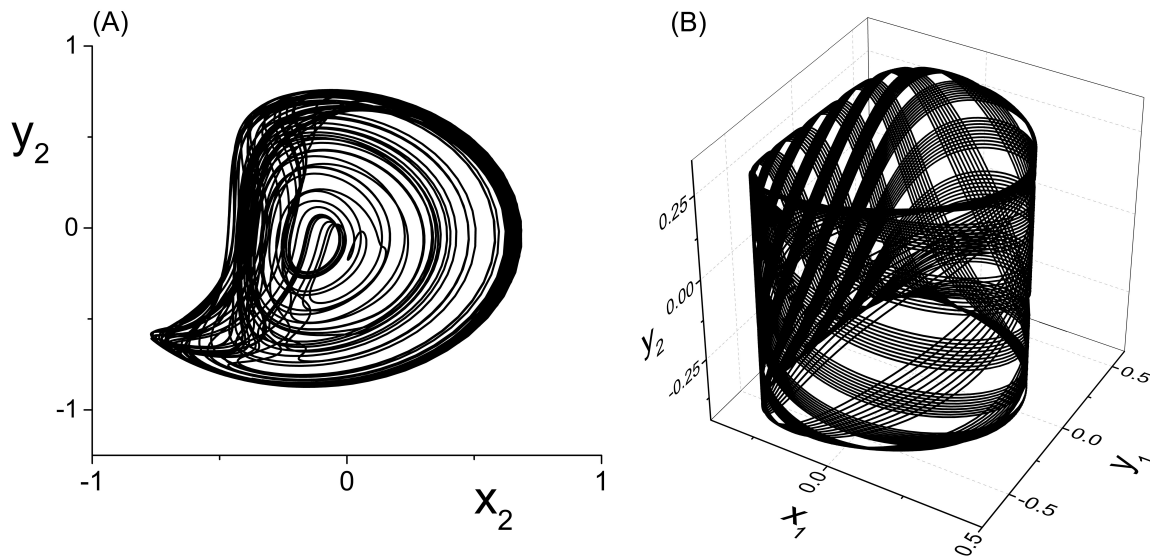


**Figure 10.** (A) Chaotic ( $y_2$  vs.  $x_2$ ) and (B) Quasiperiodic ( $y_2$  vs.  $x_1$  vs.  $y_1$ ) attractors in the response system driven by a CPW state of the driver. Parameters are:  $k_{11} = k_{22} = -9$ , with (A)  $\eta_2 = 5$ ,  $\Delta_1 = \Delta_2 = 0.5$  and  $k_{21} = 5.296$ , and (B)  $\eta_2 = 10.75$ ,  $\Delta_1 = 0.5$ ,  $\Delta_2 = 0.3$ , and  $k_{21} = 0.1$ .

304 even in this simplest of configurations, the response system (and hence, the network as a whole) can  
 305 exhibit a full range of dynamical behaviors and surprising complexity. A notable strength of our work  
 306 is that despite the complexity that emerges from this arrangement, the behavior can be understood and  
 307 explained in terms of what is known about a single population’s dynamics and bifurcation structure.

308 With the driving system on a fixed equilibrium, we showed that the response system is equivalent to  
 309 a single population with a simple shift in one parameter. Specifically, this parameter is the median of  
 310 the distribution of excitability parameters in the response system, which indicates whether the response  
 311 population is dominated by excitable or intrinsically-spiking neurons. Although this arrangement does not  
 312 introduce any new dynamical features, we showed that the response system can nevertheless still exhibit  
 313 an interesting bifurcation structure involving macroscopic equilibria, limit cycles, and multistability as  
 314 the strength of the inter-population coupling varies. More interestingly, we found that the inter-population  
 315 coupling strength is effectively equivalent to the response system’s median intra-population excitability.  
 316 By this we mean that changes in either of these rather different network parameters lead to identical  
 317 bifurcation scenarios. This surprising result follows from the drive-response network configuration in  
 318 particular.

319 The first level of additional complication arose when modestly altering an internal parameter of the drive  
 320 system. This effectively led to a *nonlinear* change in the response system’s median excitability, causing a  
 321 dramatic change in the response’s bifurcation structure. Such bifurcation structures might be difficult to  
 322 understand if encountered blindly, as might be the case when studying the dynamics of a network without  
 323 knowledge of its internal structure. Experimental studies of neuronal networks often take a similar “black  
 324 box” approach out of necessity, since detailed knowledge of connectivity (i.e., the “connectome”) is rarely  
 325 available. In our case, however, we showed that knowledge of the nonlinearity, along with knowledge of  
 326 the bifurcation structure of a single network, leads to a natural explanation of the additional features  
 327 that arise due to the network-of-networks structure. In our particular case studies, we observed multiple  
 328 distorted and reversed copies of the bifurcation structure that is associated with a single population of theta  
 329 neurons. We therefore speculate that in “black box” investigations, the observation of such repeated and/or

330 distorted bifurcation structures might be indicative of driver-response-type connectivity in the network of  
331 study.

332 Finally, we investigated the consequences of placing the driver system on a collective rhythmic state  
333 (i.e., a macroscopic periodic orbit). Our results were consistent with previous results that studied non-  
334 autonomous phase oscillator (**So and Barreto** (2011)) and theta neuron systems (**So et al.** (2014)). In those  
335 investigations, it was shown that networks of oscillators subjected to a sinusoidal variation of a network  
336 parameter led to complicated dynamics including quasiperiodicity and macroscopic chaos. Here, our  
337 driver-response arrangement of two separate interacting populations of theta neurons leads to an overall  
338 autonomous system, but with the response system being subjected to a periodic driving signal from the  
339 driver. Such arrangements might be found in real neuronal systems at the early stages of sensory input  
340 processing. For example, the lateral geniculate nucleus may be driven by a periodic visual signal delivered  
341 to the retina. Another candidate might be the trisynaptic circuit of the dentate gyrus and the CA3 and  
342 CA1 regions of the hippocampus (**Kandel et al.** (2000)). More generally, the information-processing  
343 capabilities of the brain are thought to be regulated by collective rhythms, notably theta and gamma  
344 oscillations, which arise in various areas and periodically drive other areas (**Buzsáki** (2006)).

345 Our results may also have implications for populations of bursting neurons (**So et al.** (2014)). Neuronal  
346 bursting in individual neurons is commonly understood to arise as the result of the interplay between a  
347 slowly oscillating neuronal parameter (or “slow variable”) and the neuron’s fast spiking dynamics. Bur-  
348 sting arises if the slow parameter sweeps back and forth across bifurcations, and **Rinzel and Ermentrout**  
349 (1989) classified bursters as square, parabolic, or elliptic based on the bifurcations encountered in this pro-  
350 cess. It has also been demonstrated that slowly oscillating intra- and extracellular ion concentrations can  
351 lead to wide range of neuronal bursting behaviors (**Cressman et al.** (2009, 2011); **Barreto and Cressman**  
352 (2011)).

353 Finally, we note that our explorations in this work were limited to cases in which the driver population’s  
354 parameters were either fixed or were varied only modestly. In the latter case, we changed the driver’s  
355 median excitability parameter only to the extent that its collective equilibrium state was displaced but not  
356 altered. Significantly greater complexity in the response’s dynamics would arise if the collective state of  
357 the driver were pushed across its own bifurcations, possibly resulting in topological changes and hyste-  
358 retic effects in the macroscopic driver’s state. As discussed above, such complexity would be difficult  
359 to understand if encountered in a “black box”-type investigation. Nevertheless, if it is known that the  
360 network of interest has a driver-response structure, it may be possible to comprehend the origin of such  
361 complexity in the manner that we have outlined here.

362 This study constitutes an initial attempt at building a mathematically tractable model to understand the  
363 collective behavior of a hierarchical “network-of-networks” arrangement of model neurons. In future work  
364 we plan to consider networks of networks that include feedback connections and additional populations in  
365 an effort to understand the emergence of macroscopic dynamical complexity in more realistic networks.

## AUTHOR CONTRIBUTIONS

366 TBL, EB, and PS conceived and designed the investigation, analyzed the data, and wrote the paper. TBL  
367 and PS performed the numerical computations.

## REFERENCES

368 Bacci, A., Huguenard, J. R., and Prince, D. A. (2003), Functional autaptic neurotransmission in  
369 fast-spiking interneurons: A novel form of feedback inhibition in the neocortex, *The Journal of*  
370 *Neuroscience*, 423, 3, 856–866

- 371 Barreto, E. and Cressman, J. (2011), Ion concentration dynamics as a mechanism for neuronal bursting,  
372 *Journal of Biological Physics*, 37, 3, 361–373, doi:10.1007/s10867-010-9212-6
- 373 Bekkers, J. M. (2003), Synaptic transmission: Functional autapses in the cortex, *Current Biology*, 13, 11,  
374 R433–R435, doi:10.1016/S0960-9822(03)00363-4
- 375 Bullmore, E. and Sporns, O. (2009), Complex brain network: graph theoretical analysis of structural and  
376 functional systems, *Natural Review Neuroscience*, 10, 186–198
- 377 Buzsáki, G. (2006), *Rhythms of the Brain* (Oxford University Press, New York), 1 edition
- 378 Cressman, J., Ullah, G., Ziburkus, J., Schiff, S., and Barreto, E. (2009), The influence of sodium and  
379 potassium dynamics on excitability, seizures, and the stability of persistent states: 1. Single neuron  
380 dynamics, *Journal of Computational Neuroscience*, 26, 1, 159–170
- 381 Cressman, J., Ullah, G., Ziburkus, J., Schiff, S., and Barreto, E. (2011), Erratum to: The influence  
382 of sodium and potassium dynamics on excitability, seizures, and the stability of persistent states:  
383 I. single neuron dynamics, *Journal of Computational Neuroscience*, 30, 3, 781–781, doi:10.1007/  
384 s10827-011-0333-0
- 385 Ermentrout, G. (1996), Type I membranes, phase resetting curves and synchrony, *Neural Computation*, 8,  
386 5, 979–1001
- 387 Ermentrout, G. (2002), *Simulating, Analyzing, and Animating Dynamical Systems (A Guide to XPPAUT  
388 for Researchers and Students)* (SIAM, Philadelphia, PA)
- 389 Ermentrout, G. and Kopell, N. (1986), Parabolic bursting in an excitable system coupled with a slow  
390 oscillation, *SIAM Journal on Applied Mathematics*, 46, 2, 233–253, doi:10.1137/0146017
- 391 Harris, K. (2005), Neural signatures of cell assembly organization, *Natural Review Neuroscience*, 6,  
392 399–407
- 393 Hebb, D. (1949), *The organization of behavior: a neuropsychological theory* (Wiley, New York, NY), 1  
394 edition
- 395 Hodgkin, A. (1948), The local electric charges associated with repetitive action in non-medulated axons,  
396 *Journal of Physiology*, 107, 165–181
- 397 Izhikevich, E. (2007), *Dynamical systems in neuroscience: The geometry of excitability and bursting*  
398 (MIT Press)
- 399 Kandel, E., Schwartz, J., and Jessell, T. (2000), *Principles of Neural Science* (McGraw-Hill, New York,  
400 NY), 4 edition
- 401 Laing, C. (2014), Derivation of a neural field model from a network of theta neurons, *Physical Review E*,  
402 90, 010901(R)
- 403 Luke, T., Barreto, E., and So, P. (2013), Complete classification of the macroscopic behavior of a  
404 heterogeneous network of theta neurons, *Neural Computation*, 25, 12, 3207–3234, doi:10.1162/  
405 NECO\_a\_00525
- 406 Marvel, S. A., Mirollo, R. E., and Strogatz, S. H. (2009), Identical phase oscillators with global sinusoidal  
407 coupling evolve by mbius group action, *Chaos: An Interdisciplinary Journal of Nonlinear Science*, 19,  
408 4, 043104, doi:http://dx.doi.org/10.1063/1.3247089
- 409 Meunier, D., Lambiotte, R., and Bullmore, E. (2010), Modular and hierarchically modular organization  
410 of brain networks, *Frontiers in Neuroscience*, 4, 1–11
- 411 Nowak, L., Azouz, R., Sanchez-Vives, M., Gray, C., and McCormick, D. (2003), Electrophysiological  
412 classes of cat primary visual cortical neurons in vivo as revealed by quantitative analyses, *Journal of  
413 Neurophysiology*, 89, 1541–1566
- 414 Ott, E. and Antonsen, T. (2008), Low dimensional behavior of large systems of globally coupled  
415 oscillators, *Chaos*, 18, 3, doi:10.1063/1.2930766, 037113
- 416 Ott, E. and Antonsen, T. (2009), Long time evolution of phase oscillator systems, *Chaos*, 19, 2, doi:10.  
417 1063/1.3136851, 023117
- 418 Ott, E., Hunt, B. R., and Antonsen, T. M. (2011), Comment on long time evolution of phase oscillator  
419 systems [chaos 19, 023117 (2009)], *Chaos: An Interdisciplinary Journal of Nonlinear Science*, 21, 2,  
420 025112, doi:http://dx.doi.org/10.1063/1.3574931
- 421 Pazó, D. and Montbrió, E. (2014), Low-dimensional dynamics of populations of pulse-coupled oscillators,  
422 *Phys. Rev. X*, 4, 011009, doi:10.1103/PhysRevX.4.011009

- 423 Pikovsky, A. and Rosenblum, M. (2011), Dynamics of heterogeneous oscillator ensembles in terms of  
424 collective variables, *Physica D: Nonlinear Phenomena*, 240, 910, 872 – 881, doi:http://dx.doi.org/10.  
425 1016/j.physd.2011.01.002
- 426 Rinzel, J. and Ermentrout, G. (1989), Analysis of neural excitability and oscillations, in C. Koch and  
427 I. Segev, eds., *Methods in Neuronal Modeling* (The MIT Press, Cambridge, MA)
- 428 Sherrington, C. (1906), *The integrative action of the nervous system* (Scribners, New York, NY), 1 edition
- 429 So, P. and Barreto, E. (2011), Generating macroscopic chaos in a network of globally coupled phase  
430 oscillators, *Chaos*, 21, 3, doi:10.1063/1.3638441, 033127
- 431 So, P., Luke, T., and Barreto, E. (2014), Networks of theta neurons with time-varying excitability: Macro-  
432 scopic chaos, multistability, and final-state uncertainty, *Physica D*, 267, 16–26, doi:10.1016/j.physd.  
433 2013.04.009
- 434 Tateno, T., Harsch, A., and Robinson, H. (2004), Threshold firing frequency-current relationships of  
435 neurons in rat somatosensory cortex: Type 1 and type 2 dynamics, *Journal of Neurophysiology*, 92,  
436 2283–2294
- 437 Zhou, C., Zemanova, L., Zamora, G., Hilgetag, C., and Kurths, J. (2006), Hierarchical organization  
438 unveiled by functional connectivity in complex brain networks, *Physical Review Letters*, 97, 238103

## FIGURES

Figure 1.JPEG

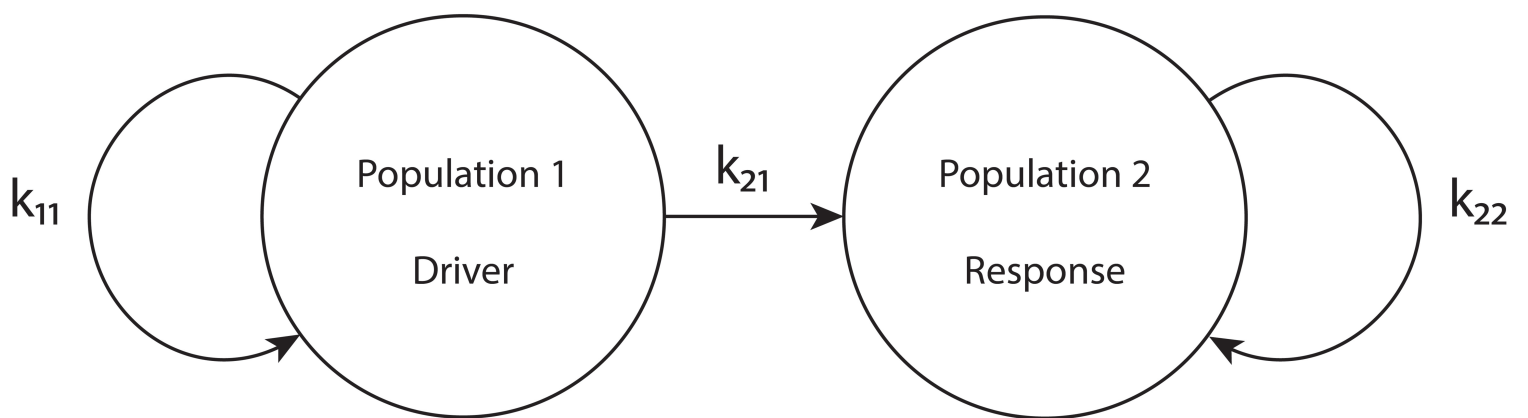


Figure 2.JPEG

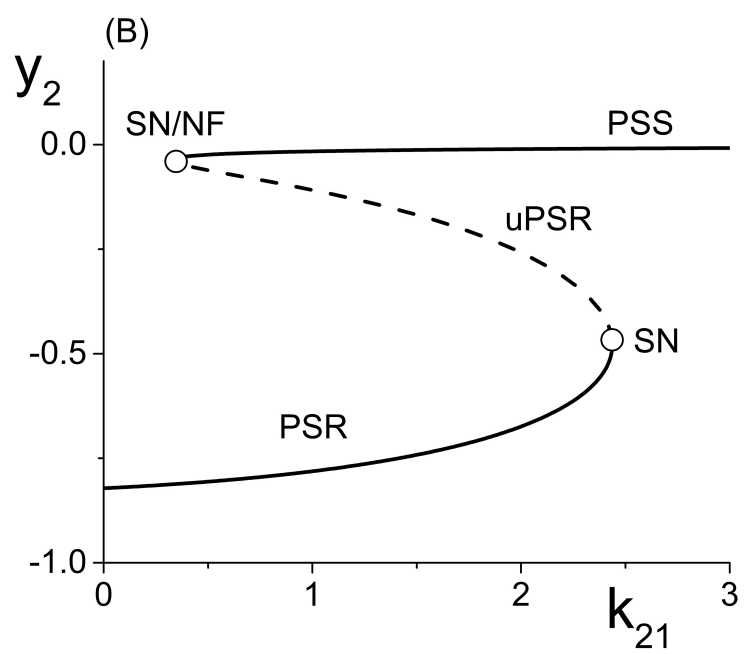
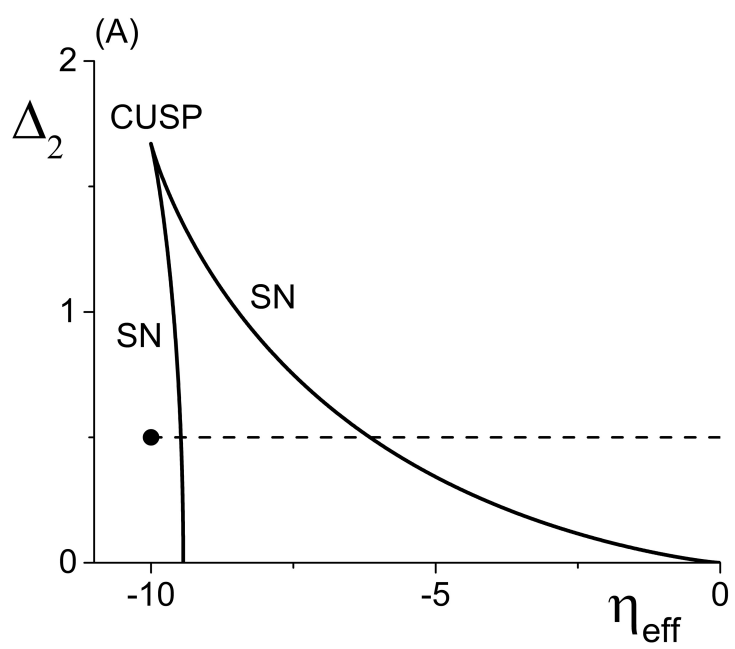


Figure 3.JPEG

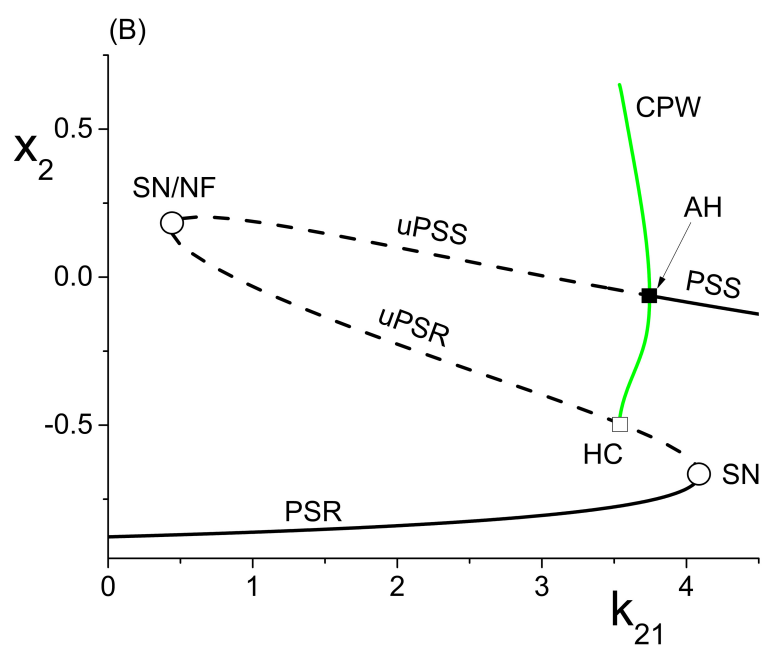
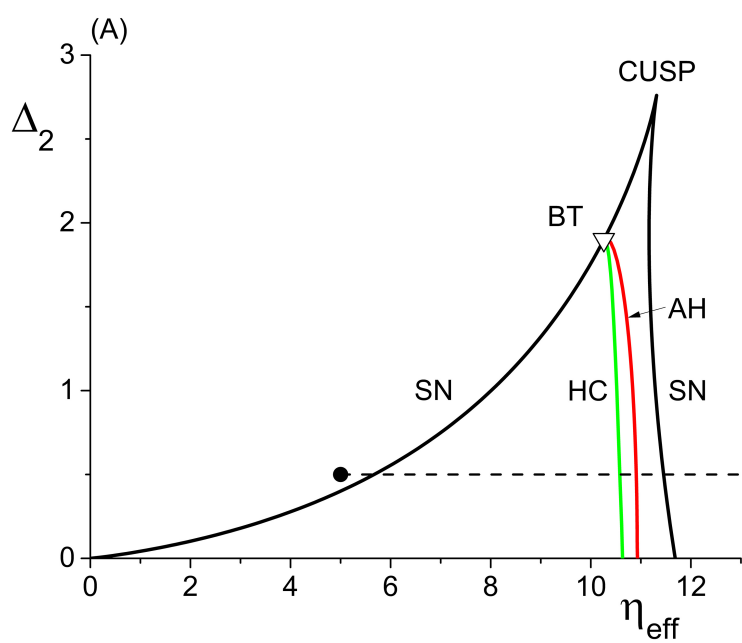


Figure 4.JPEG

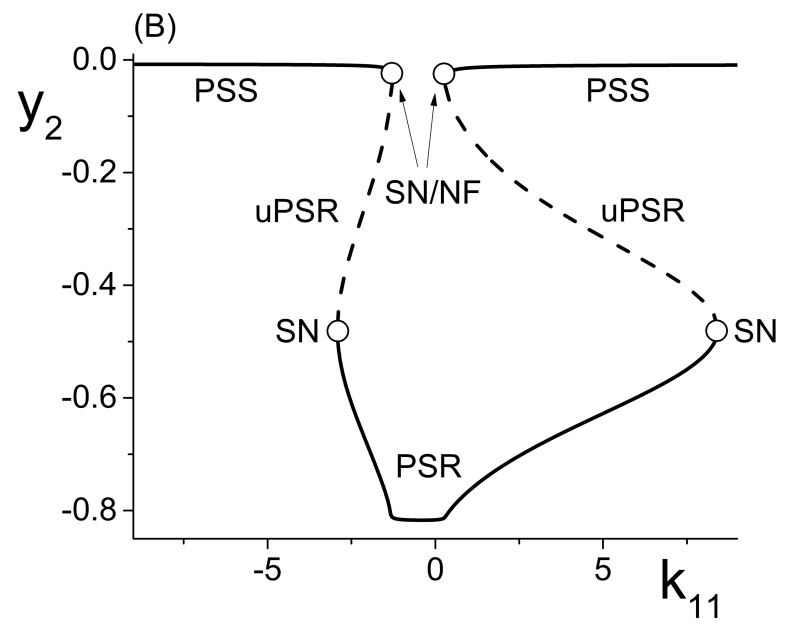
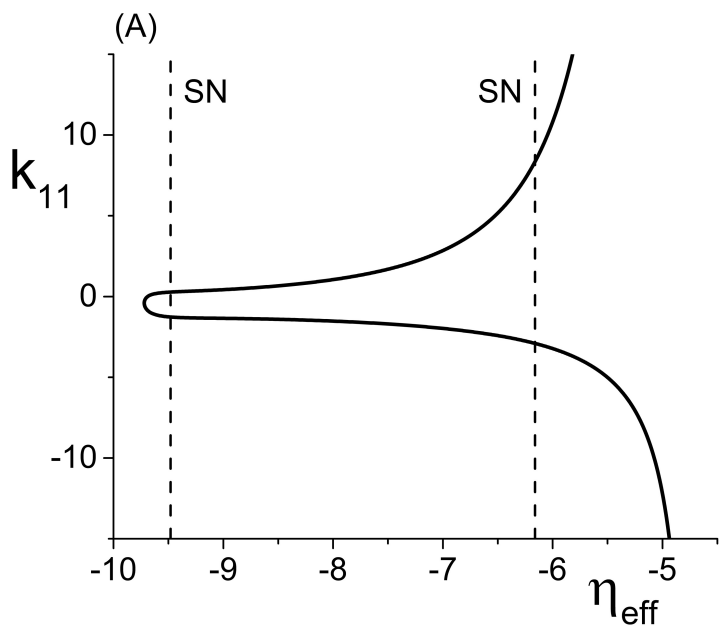


Figure 5.JPEG

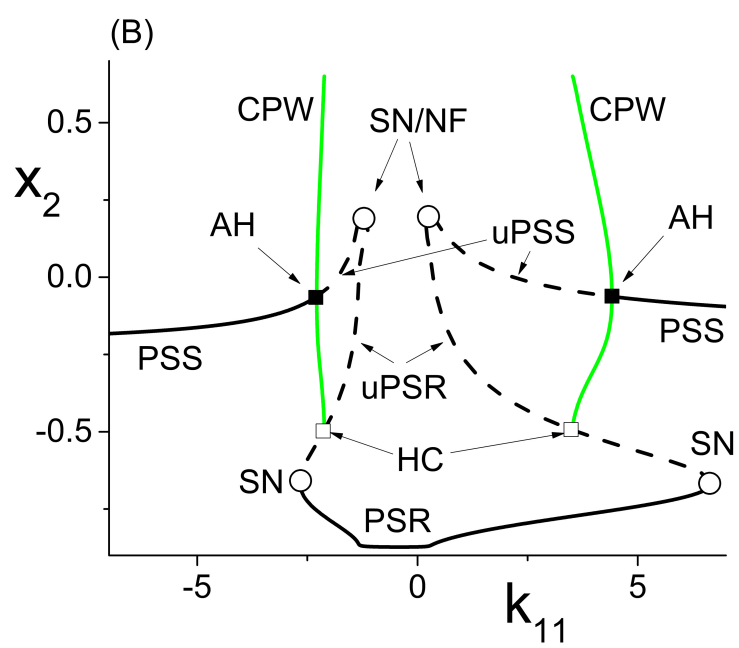
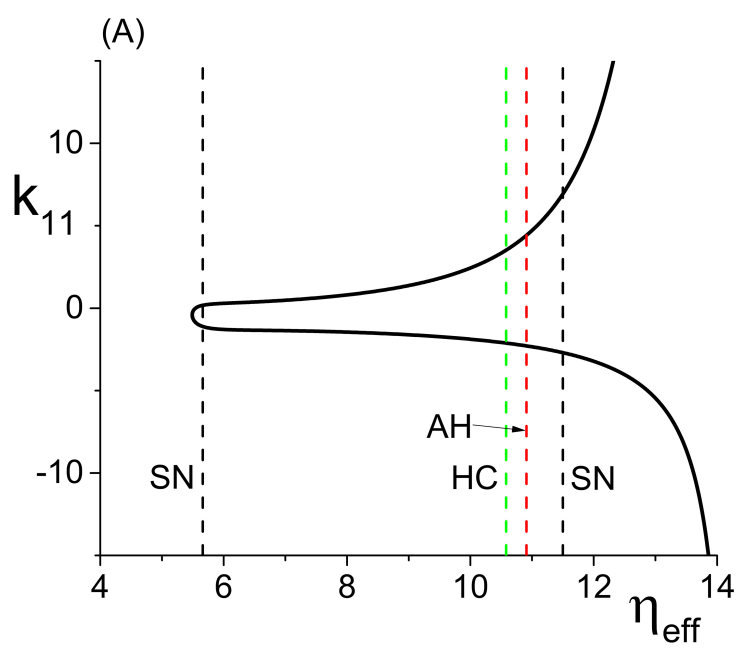


Figure 6.JPEG

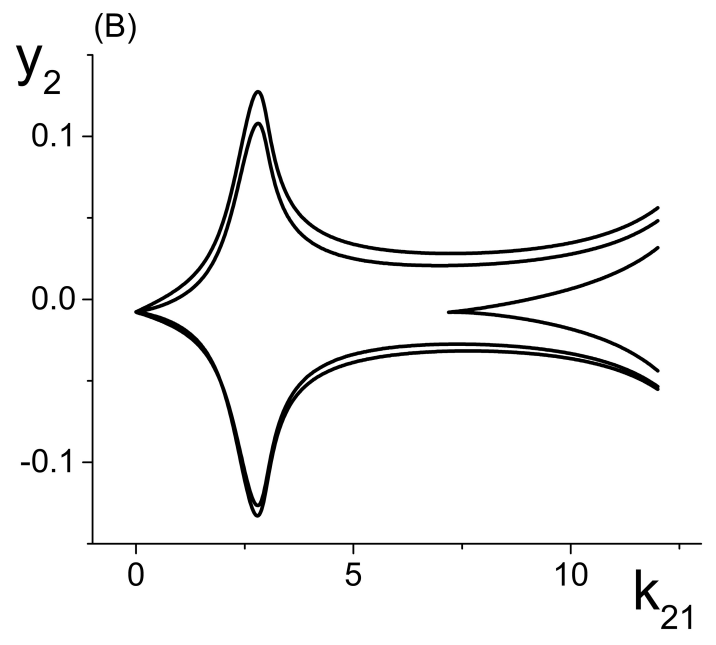
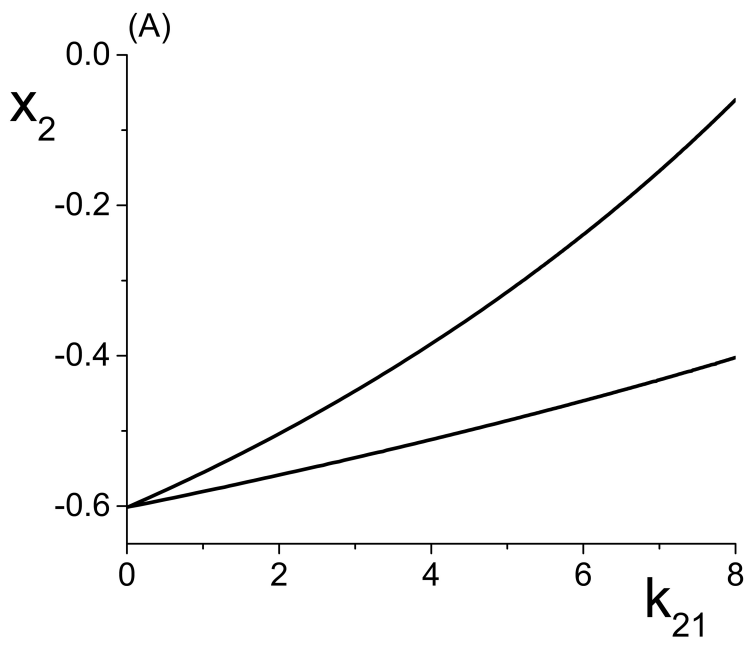


Figure 7.JPEG

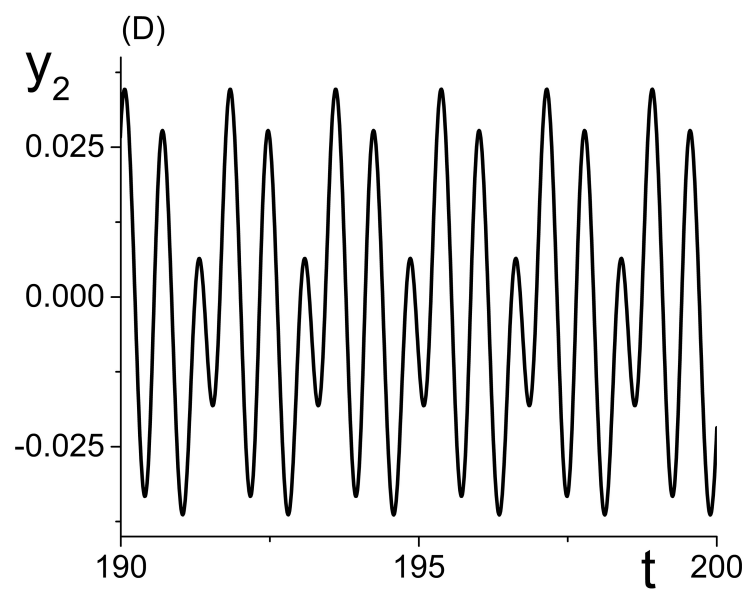
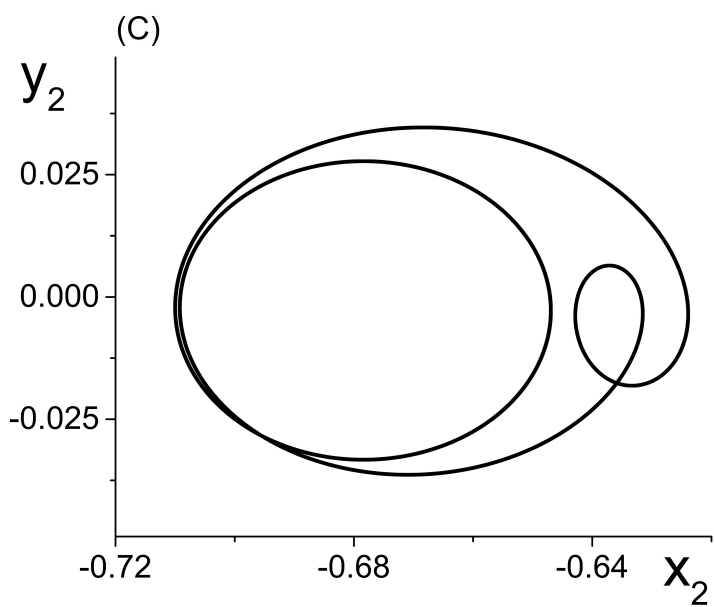
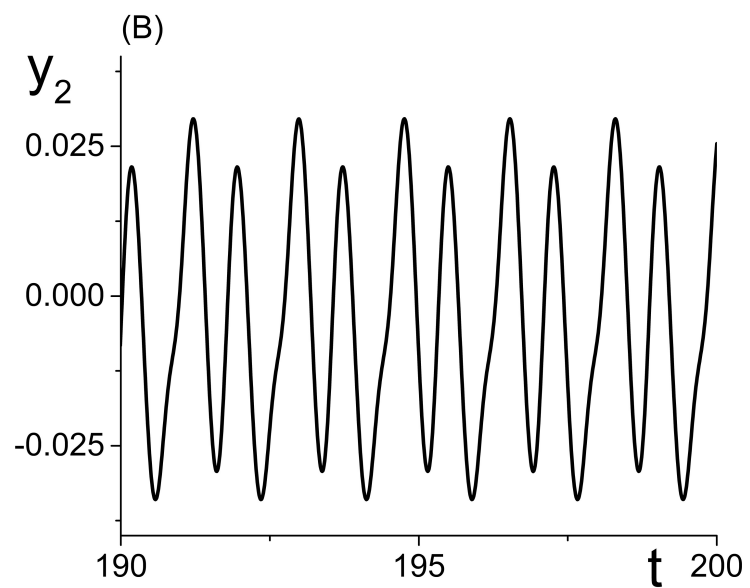
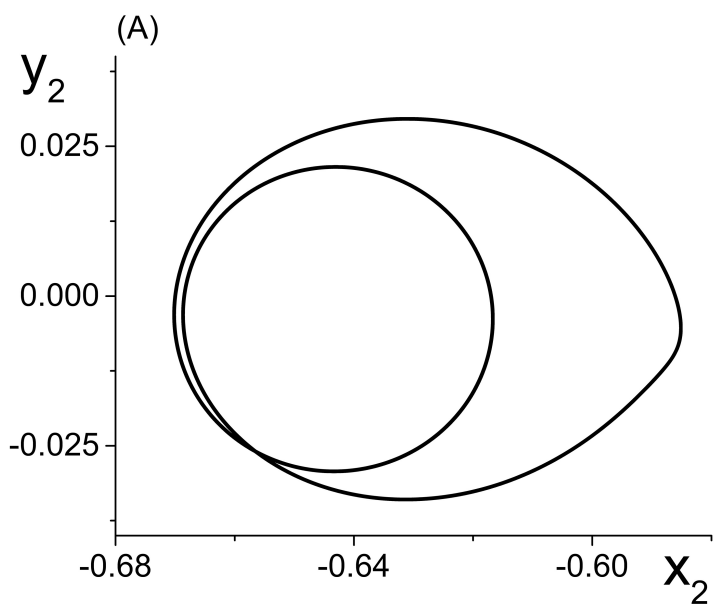


Figure 8.JPEG

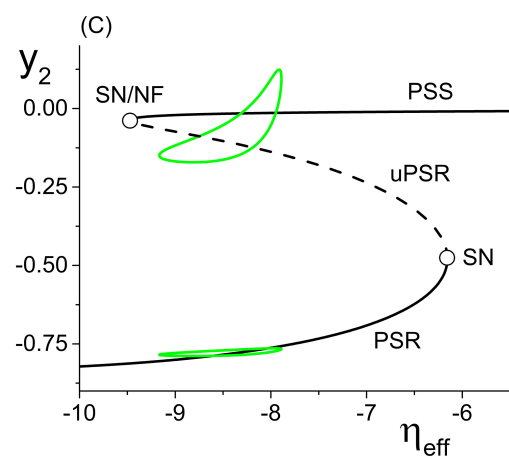
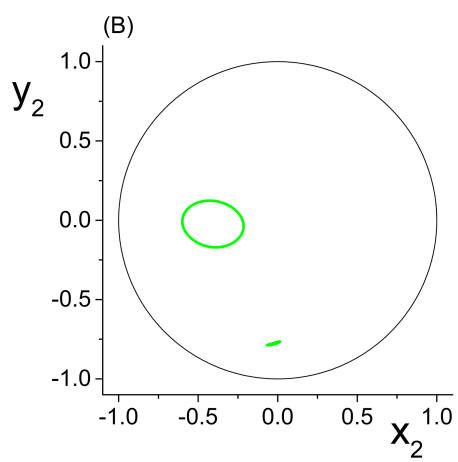
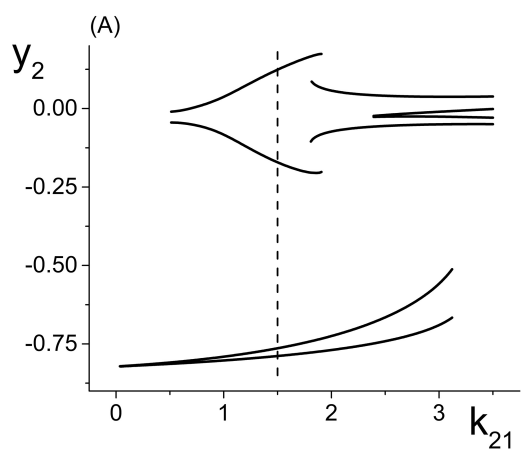


Figure 9.JPEG

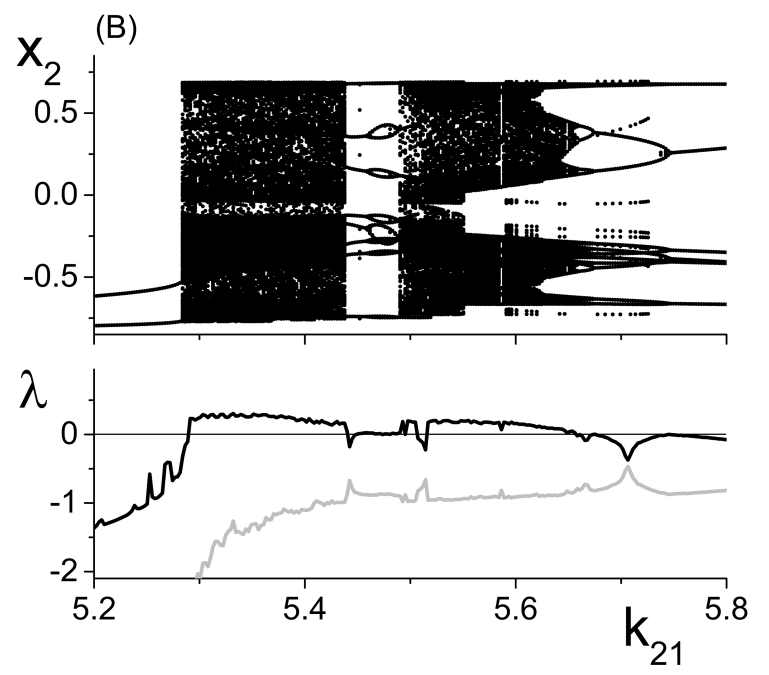
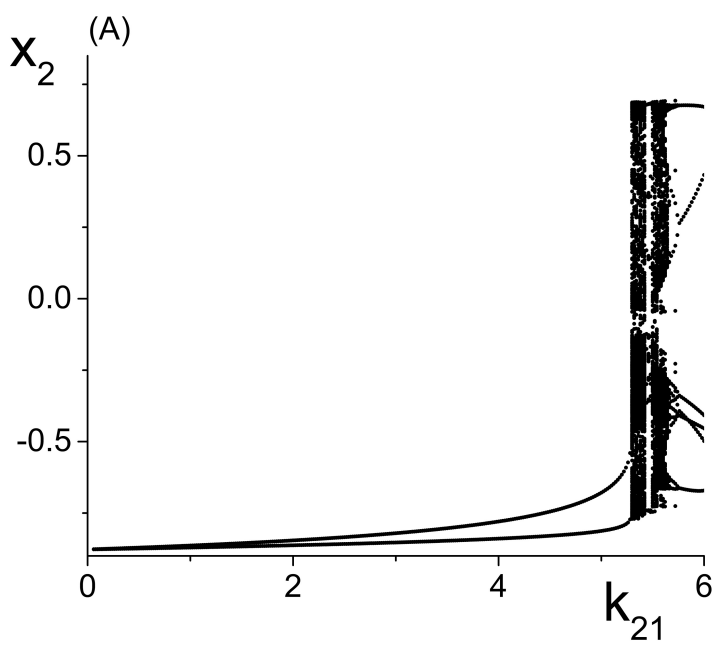


Figure 10.JPEG

